Measurement of the inclusive charm cross section at 4.03 GeV and 4.14 GeV

J. Z. Bai,[1] Y. Ban,[5] J. G. Bian,[1] I. Blum,[12] G. P. Chen,[1] H. F. Chen,[11] J. Chen,[3] J. C. Chen,[1] Y. Chen,[1] Y. B. Chen,[1] Y. Q. Chen,[1] B. S. Cheng,[1] X. Z. Cui,[1] H. L. Ding,[1] L. Y. Dong,[1] Z. Z. Du,[1] W. Dunwoodie,[8] C. S. Gao,[1] M. L. Gao,[1] S. Q. Gao,[1] P. Gratton,[12] J. H. Gu,[1] S. D. Gu,[1] W. X. Gu,[1] Y. F. Gu,[1] Y. N. Guo,[1] Z. J. Guo,[1] S. W. Han,[1] Y. Han,[1] F. A. Harris,[9] J. He,[1] J. T. He,[1] K. L. He,[1] M. He,[6] Y. K. Heng,[1] D. G. Hitlin,[2] G. Y. Hu,[1] H. M. Hu,[1] J. L. Hu,[1] Q. H. Hu,[1] T. Hu,[1] X. Q. Hu,[1] Y. Z. Huang,[1] G. S. Huang,[1] J. M. Izen,[12] C. H. Jiang,[1] Y. Jin,[1] B. D. Jones,[12] X. Ju,[1] Z. J. Ke,[1] M. H. Kelsey,[2] B. K. Kim,[12] D. Kong,[9] Y. F. Lai,[1] P. F. Lang,[1] A. Lankford,[10] C. G. Li,[1] D. Li,[1] H. B. Li,[1] J. Li,[1] J. C. Li,[1] P. Q. Li,[1] R. B. Li,[1] W. Li,[1] W. G. Li,[1] X. H. Li,[1] X. N. Li,[1] H. M. Liu,[1] J. Liu,[1] R. G. Liu,[1] Y. Liu,[1] X. C. Lou,[12] B. Lowery,[12] F. Lu,[1] J. G. Lu,[1] X. L. Luo,[1] E. C. Ma,[1] J. M. Ma,[1] R. Malchow,[3] M. Mandelkern,[10] H. S. Mao,[1] Z. P. Mao,[1] X. C. Meng,[1] J. Nie,[1] S. L. Olsen,[9] J. Oyang,[2] D. Paluselli,[9] L. J. Pan,[9] J. Panetta,[2] F. Porter,[2] N. D. Qi,[1] X. R. Qi,[1] C. D. Qian,[7] J. F. Qiu,[1] Y. H. Qu,[1] Y. K. Que,[1] G. Rong,[1] M. Schernau,[10] B. Schmid,[10] J. Schultz,[10] Y. Y. Shao,[1] B. W. Shen,[1] D. L. Shen,[1] H. Shen,[1] X. Y. Shen,[1] H. Y. Sheng,[1] H. Z. Shi,[1] X. F. Song,[1] J. Standifird,[12] D. Stoker,[10] F. Sun,[1] H. S. Sun,[1] Y. Sun,[1] Y. Z. Sun,[1] S. Q. Tang,[1] W. Toki,[3] G. L. Tong,[1] G. S. Varner,[9] F. Wang,[1] L. S. Wang,[1] L. Z. Wang,[1] M. Wang,[1] P. Wang,[1] P. L. Wang,[1] S. M. Wang,[1] T. J. Wang,[1,*] Y. Y. Wang,[1] M. Weaver,[2] C. L. Wei,[1] N. Wu,[1] Y. G. Wu,[1] D. M. Xi,[1] X. M. Xia,[1] P. P. Xie,[1] Y. Xie,[1] Y. H. Xie,[1] G. F. Xu,[1] S. T. Xue,[1] J. Yan,[1] W. G. Yan,[1] C. M. Yang,[1] C. Y. Yang,[1] H. X. Yang,[1] J. Yang,[1] W. Yang,[3] X. F. Yang,[1] M. H. Ye,[1] S. W. Ye,[11] Y. X. Ye,[11] C. S. Yu,[1] C. X. Yu,[1] G. W. Yu,[1] Y. H. Yu,[4] Z. Q. Yu,[1] C. Z. Yuan,[1] Y. Yuan,[1] B. Y. Zhang,[1] C. Zhang,[1] C. C. Zhang,[1] D. H. Zhang,[1] Dehong Zhang,[1] H. L. Zhang,[1] J. Zhang,[1] J. W. Zhang,[1] L. Zhang,[1] L. S. Zhang,[1] P. Zhang,[1] Q. J. Zhang,[1] S. Q. Zhang,[1] X. Y. Zhang,[6] Y. Y. Zhang,[1] D. X. Zhao,[1] H. W. Zhao,[1] Jiawei Zhao,[11] J. W. Zhao,[1] M. Zhao,[1] W. R. Zhao,[1] Z. G. Zhao,[1] J. P. Zheng,[1] L. S. Zheng,[1] Z. P. Zheng,[1] B. Q. Zhou,[1] G. P. Zhou,[1] H. S. Zhou,[1] L. Zhou,[1] K. J. Zhu,[1] Q. M. Zhu,[1] Y. C. Zhu,[1] Y. S. Zhu,[1] and B. A. Zhuang[1]

(BES Collaboration)

[1]*Institute of High Energy Physics, Beijing 100039, People's Republic of China*
[2]*California Institute of Technology, Pasadena, California 91125*
[3]*Colorado State University, Fort Collins, Colorado 80523*
[4]*Hangzhou University, Hangzhou 310028, People's Republic of China*
[5]*Peking University, Beijing 100871, People's Republic of China*
[6]*Shandong University, Jinan 250100, People's Republic of China*
[7]*Shanghai Jiaotong University, Shanghai 200030, People's Republic of China*
[8]*Stanford Linear Accelerator Center, Stanford, California 94309*
[9]*University of Hawaii, Honolulu, Hawaii 96822*
[10]*University of California at Irvine, Irvine, California 92717*
[11]*University of Science and Technology of China, Hefei 230026, People's Republic of China*
[12]*University of Texas at Dallas, Richardson, Texas 75083-0688*

(Received 11 October 1999; published 2 June 2000)

The cross section for charmed meson production at $\sqrt{s}=4.03$ and 4.14 GeV has been measured with the Beijing Spectrometer. The measurement was made using 22.3 pb^{-1} of e^+e^- data collected at 4.03 GeV and 1.5 pb^{-1} of e^+e^- data collected at 4.14 GeV. Inclusive observed cross sections for the production of charged and neutral D mesons and momentum spectra are presented. Observed cross sections were radiatively corrected to obtain tree level cross sections. Measurements of the total hadronic cross section are obtained from the charmed meson cross section and an extrapolation of results from below the charm threshold.

PACS number(s): 13.65.+i, 13.85.Lg, 13.85.Ni

I. INTRODUCTION

The hadronic cross section of e^+e^- at all energies is needed to calculate the effects of vacuum polarization on parameters of the standard model. The energy region which contributes the largest uncertainty is the charm threshold region where the hadronic cross section has only been measured with an accuracy of 15–20% [1]. Traditionally, σ_{hadron} is measured by counting hadronic events. This method requires a detailed understanding of trigger conditions, the efficiency of hadronic event selection criteria, and a subtraction of two photon events and other backgrounds. An alternative is measuring σ_{charm} and adding this to an extrapolation of the $\sigma_{u,d,s}$ contribution from the region below charm threshold. The charmed mesons used in this study are the D^0 and D^+. The D_s cross sections are taken from earlier works. There is no evidence for continuum charmonium production [2]. The charm counting method is intrinsically less sensitive to trigger conditions, beam-related backgrounds, and two photon backgrounds due to the distinctive topology of charmed meson events.

*Deceased.

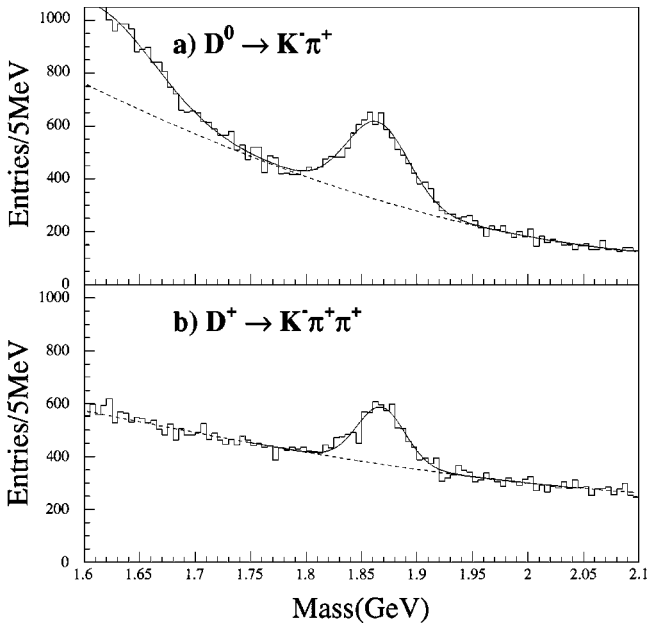

FIG. 1. The invariant mass of (a) $K\pi$ and (b) $K\pi\pi$ tags with a momentum between 0 and 1 GeV at $E_{c.m.}=4.03$ GeV.

II. DATA SELECTION

The data used for this analysis were accumulated with the Beijing Spectrometer [3]; the total integrated luminosity at 4.03 (4.14) GeV was 22.3 (1.5) pb^{-1}. Candidate tracks were required to have a good track fit passing within 1.5 cm of the collision point in R and 15 cm in z, and satisfying $|\cos\theta|<0.85$. Particle identification was provided by an array of time of flight (TOF) scintillation counters and specific ionization measurements in the drift chamber used for charged particle tracking (dE/dx). For pions, consistency $[CL(\pi)>0.1\%]$ and loose electron rejection $[L_\pi/(L_\pi+L_e)>0.2]$ were required, where L_X is the likelihood for hypothesis X. Kaon identification required consistency $[CL(K)>0.1\%]$, pion rejection $[L_K/(L_K+L_\pi)>0.5]$ and loose electron rejection $[L_K/(L_K+L_e)>0.2]$. Multiple counting of D^0 candidates was removed by positively identifying pions using the selection $[L_K/(L_K+L_\pi)<0.5]$. Muons are rejected using a momentum dependent criteria based on track penetration into the muon detector.

TABLE I. Number of inclusive signal events for each mode.

Mode	$E_{c.m.}$ (GeV)	Events
$D^0\to K^-\pi^+$	4.03	4174 ± 163
$D^+\to K^-\pi^+\pi^+$	4.03	2341 ± 138
$D^0\to K^-\pi^+$	4.14	249 ± 36
$D^+\to K^-\pi^+\pi^+$	4.14	126 ± 31

III. D^0 AND D^+ SIGNAL

Inclusive $K^-\pi^+$ and $K^-\pi^+\pi^+$ invariant mass distributions are shown in Figs. 1 and 2 for 4.03 and 4.14 GeV, respectively. (Here and throughout this paper, reference to a state also implies its charge conjugate state.) Each histogram was fit to a function which included a Gaussian signal plus a background function. For the $K\pi$ distributions [Figs. 1(a) and 2(a)], the background function consisted of a Gaussian centered at 1.60 GeV to account for the contribution to the $K\pi$ spectrum from $D^0\to K\pi\pi^0$ decays plus a third order polynomial background. For the $K\pi\pi$ distributions [Figs. 1(b) and 2(b)], the background function consisted of a third order polynomial. The number of signal events in each mode is given in Table I.

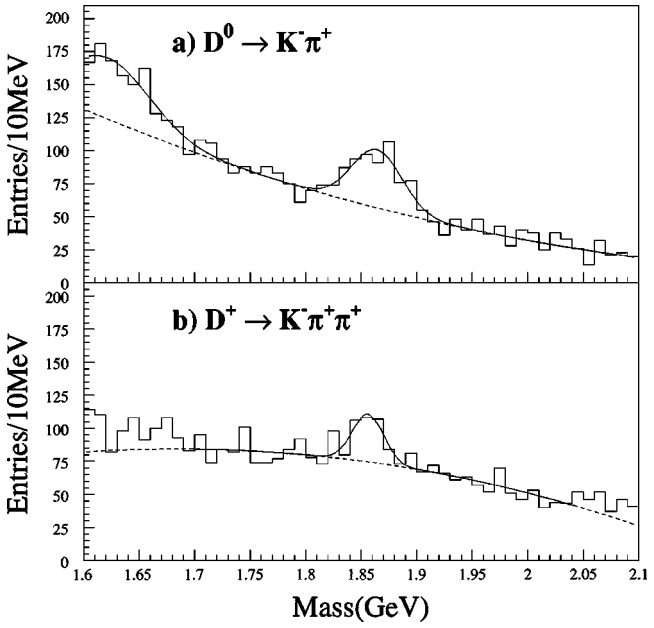

FIG. 2. The invariant mass of (a) $K\pi$ and (b) $K\pi\pi$ tags with a momentum between 0 and 1 GeV at $E_{c.m.}=4.14$ GeV.

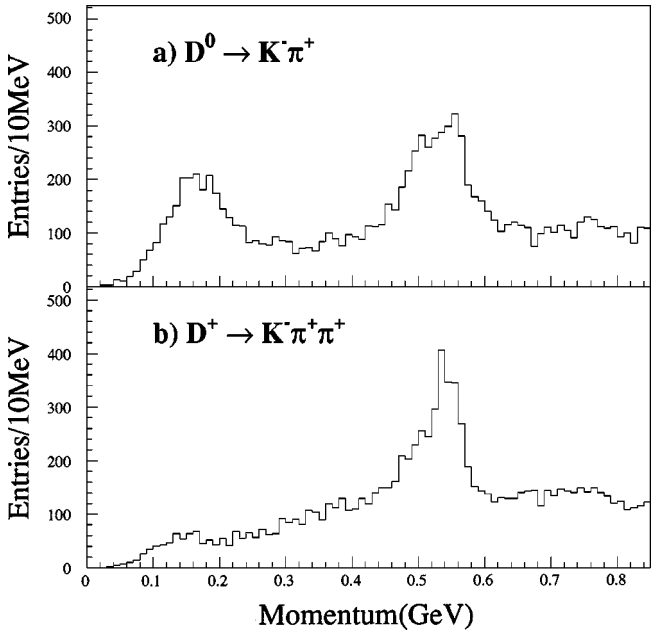

FIG. 3. The momentum of (a) $K\pi$ and (b) $K\pi\pi$ tags with a mass between 1.81 and 1.91 GeV at $E_{c.m.}=4.03$ GeV.

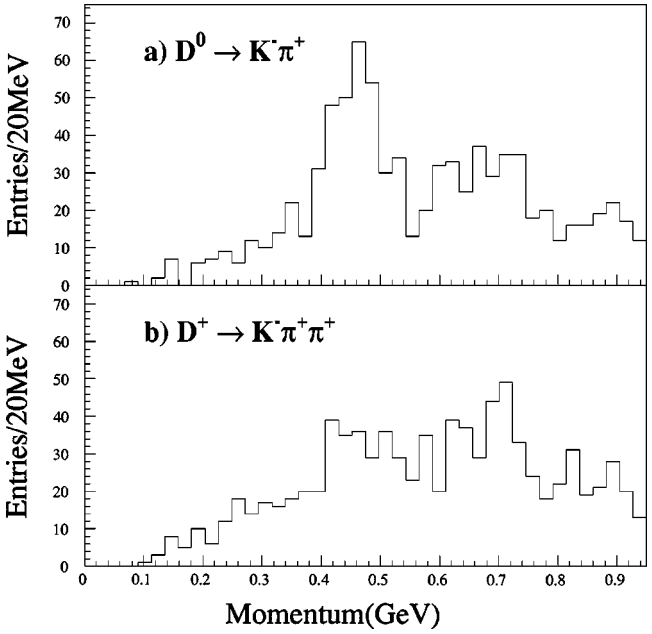

FIG. 4. The momentum of (a) $K\pi$ and (b) $K\pi\pi$ tags with a mass between 1.82 and 1.92 GeV at $E_{c.m.}=4.14$ GeV.

The momentum spectra of D candidates with a mass between 1.81 and 1.91 GeV is presented in Fig. 3 for $\sqrt{s}=4.03$ GeV. The three momentum regions near 0.15, 0.55, and 0.75 GeV correspond to $D^*\bar{D}^*$, $D^*\bar{D}$, and $D\bar{D}$ production, respectively. The spectrum for $\sqrt{s}=4.14$ GeV is shown in Fig. 4. The momentum regions near 0.45 and 0.70 and 0.90 GeV correspond to $D^*\bar{D}^*$, $D^*\bar{D}$, and $D\bar{D}$ production, respectively. The shapes of the $D^*\bar{D}^*$ spectrum and part of the $D^*\bar{D}$ spectrum are broadened due to Doppler-smeared D mesons coming from D^* decays. In addition, a small low momentum tail on each structure is expected due to initial state radiation. The background shape under the momentum spectrum is not flat, making a direct subtraction difficult.

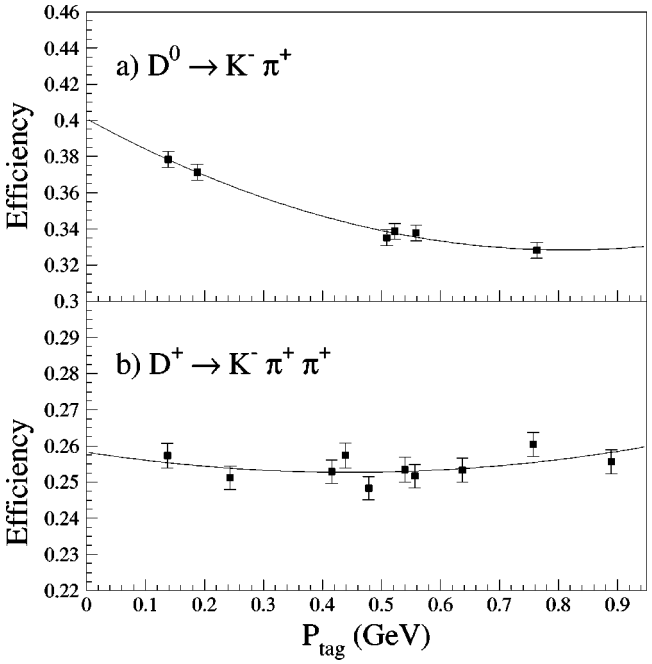

FIG. 5. The momentum dependence of the reconstruction efficiency.

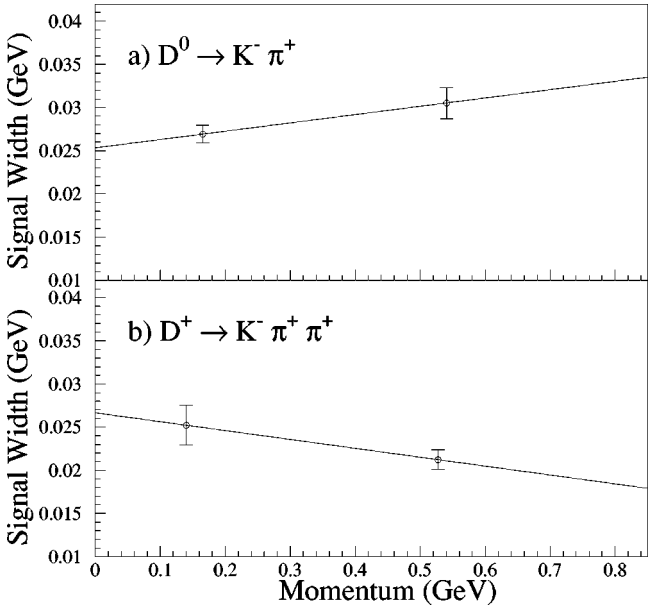

FIG. 6. The momentum dependence of the mass resolution.

IV. CROSS SECTION

If the reconstruction efficiency for D mesons were constant with respect to momentum, the observed cross section could be determined using

$$\sigma(e^+e^-\to DX)=\frac{N_{(\text{signal})}}{\epsilon B\mathcal{L}}, \tag{1}$$

where N(signal) is the number of signal events, ϵ is the efficiency, B is the branching fraction of the D meson to a decay mode and $\mathcal{L}$ is the luminosity. However, Monte Carlo studies show some momentum dependence to the reconstruc-

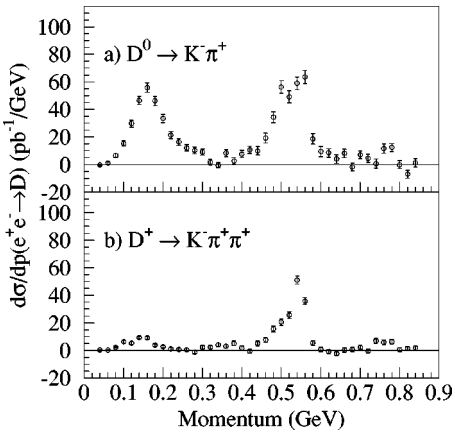

FIG. 7. The differential production cross section of (a) $e^+e^-\to D^0X$ and (b) $e^+e^-\to D^+X$ versus the momentum of the reconstructed D at $E_{c.m.}=4.03$ GeV.

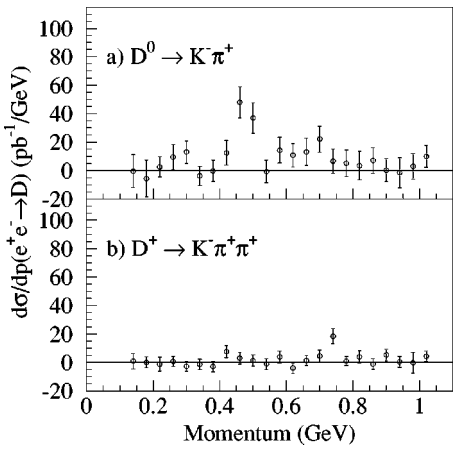

FIG. 8. The differential production cross section of (a) $e^+e^- \to D^0X$ and (b) $e^+e^- \to D^+X$ versus the momentum of the reconstructed D at $E_{c.m.} = 4.14$ GeV.

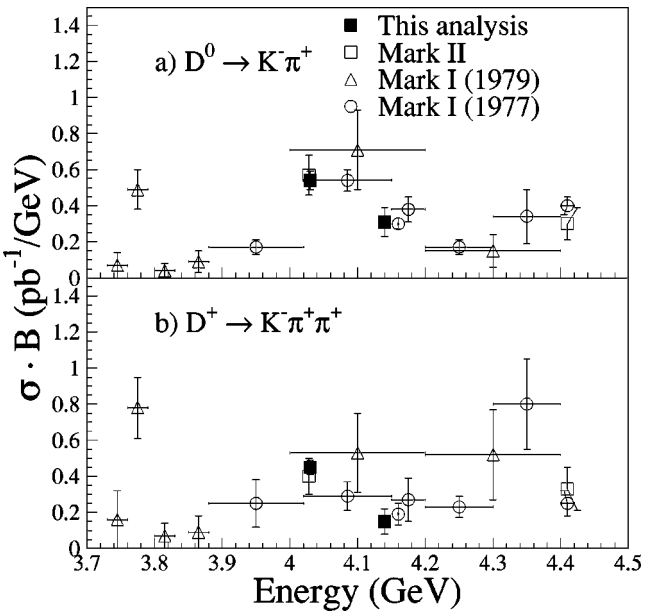

FIG. 9. Comparison of the observed integrated cross section times branching fraction for this analysis with those of Mark I and Mark II. (a) $D^0 \to K\pi$; (b) $D^+ \to K\pi\pi$.

tion efficiency (Fig. 5). In order to measure the cross section, the momentum spectrum for D^0 and D^+ mesons from 50 to 850 (110 to 1030) MeV was divided into 20 (40) MeV slices for 4.03 (4.14) GeV data. For each momentum slice, the invariant mass distribution was fit with a Gaussian plus a polynomial background. The central value of the Gaussian was fixed at the nominal D mass; the width was fixed to a momentum dependent value determined by a fit to a coarser slicing of the data (Fig. 6). The differential cross section with respect to momentum for this data is shown in Figs. 7 and 8 for 4.03 and 4.14 GeV, respectively. The cross section times branching fractions of D^0 and D^+ mesons and cross sections calculated using the branching fractions of Ref. [4] are shown in Table II. The $\sigma \cdot B$ values from this measurement are compatible with previous measurements by Mark I [5,6] and Mark II [7] as shown in Fig. 9.

V. CORRECTIONS FOR INITIAL STATE RADIATION

The tree level cross sections for charm at $\sqrt{s} = 4.03$ GeV and $\sqrt{s} = 4.14$ GeV were obtained by correcting the observed cross section for the effects of initial state radiation (ISR). The ISR correction is dependent on the cross section for all energies less than the nominal energy. Since these measurements were performed only at two energies, some theoretical modeling of the cross section distribution was required. Two different theoretical predictions for these cross sections were used in this analysis, the coupled channel model [8], and a P-wave phase space formalism. The models provide predictions for $\sigma_{B,i}(s_{\rm eff})$, the tree level (Born) cross section as a function of the effective center of mass energy squared for production mode i, where $i = D^0\overline{D}^0$, D^+D^-, $D^{*0}\overline{D}^0$, $D^{*+}D^-$, $D^{*0}\overline{D}^{*0}$, $D^{*+}D^{*-}$. The effective center of mass energy squared is given by

$$s_{\rm eff} \equiv s_{\rm nom}(1-k), \tag{2}$$

where $k \cdot E_{\rm beam}$ is the energy of radiated photons and $s_{\rm nom}$ is the nominal center of mass energy squared. The tree level cross sections are convoluted with a sampling function $f(k, s_{\rm nom})$ that represents a first order calculation of the effective luminosity for radiated photons in a two body radiation model [9], giving the observed cross section at $s_{\rm nom}$:

$$\sigma_{{\rm obs},i}(s_{\rm nom}) = \int_0^1 dk \cdot f(k, s_{\rm nom}) \sigma_{B,i}(s_{\rm eff})(1 + \delta_{VP}(s_{\rm eff})). \tag{3}$$

The vacuum polarization correction $(1 + \delta_{VP})$ includes both leptonic and hadronic terms. It varies from charm threshold to 4.14 GeV by less than $\pm 2\%$. It is treated as a constant with the value

$$(1 + \delta_{VP}) = 1.047 \pm 0.024 \tag{4}$$

TABLE II. The observed cross section times branching fraction of D^0 and D^+ and the observed cross section of D^0 and D^+ at 4.03 GeV and 4.14 GeV.

	$\sqrt{s} = 4.03$ GeV	$\sqrt{s} = 4.14$ GeV
$(\sigma_{D^0} + \sigma_{\overline{D}^0}) \cdot B(D^0 \to K^-\pi^+)$	$0.537 \pm 0.015 \pm 0.047$ nb	$0.31 \pm 0.07 \pm 0.03$ nb
$(\sigma_{D^+} + \sigma_{D^-}) \cdot B(D^+ \to K^-\pi^+\pi^+)$	$0.449 \pm 0.017 \pm 0.036$ nb	$0.15 \pm 0.07 \pm 0.01$ nb
$\sigma_{D^0} + \sigma_{\overline{D}^0}$	$13.9 \pm 0.4 \pm 1.3$ nb	$8.1 \pm 1.8 \pm 0.7$ nb
$\sigma_{D^+} + \sigma_{D^-}$	$5.0 \pm 0.2 \pm 0.5$ nb	$1.7 \pm 0.8 \pm 0.2$ nb

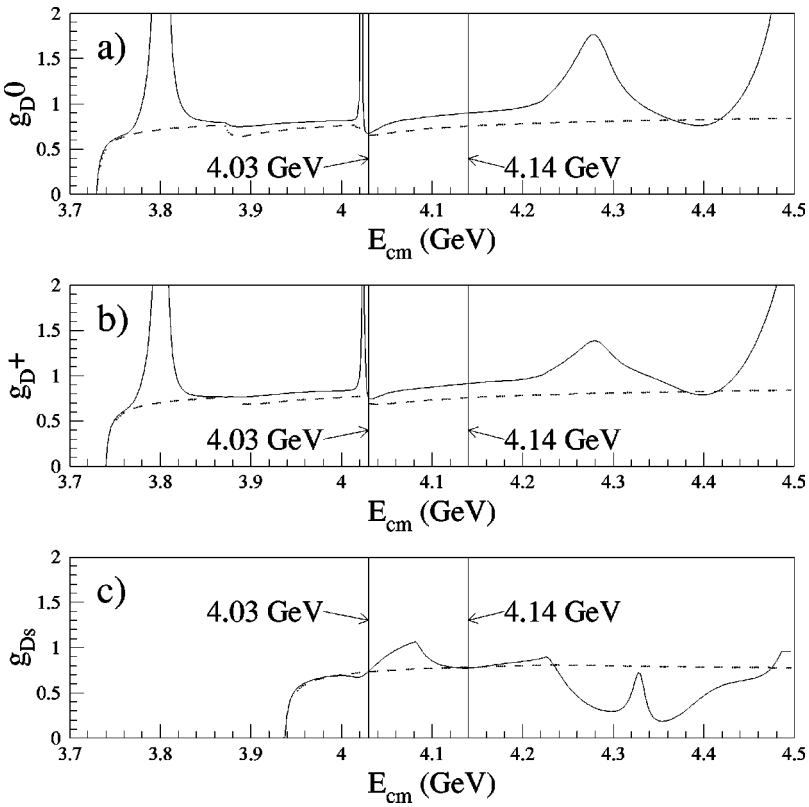

FIG. 10. The ISR correction for (a) D^0, (b) D^+, and (c) D_s. The correction using the coupled channel model is solid, while the *p*-wave phase space formalism is dashed.

and moved outside the integrand. With this simplification, the ISR correction, $g_i(s_{\rm nom})$, is defined by

$$g_i(s_{\rm nom}) \equiv \frac{\sigma_{{\rm obs},i}(s_{\rm nom})}{\sigma_{B,i}(s_{\rm nom})(1+\delta_{VP})}. \tag{5}$$

The D^{*0} and D^{*+} branching fractions are used to calculate $N_{D^0,i}$ and $N_{D^+,i}$, the mean number of D^0 and D^+ per production mode i event. The $N_{D^0,i}$ and $N_{D^+,i}$ values are used to weight the ISR correction for each mode to obtain the ISR correction averaged over all production modes:

$$g_{D^0}(s_{\rm nom}) = \frac{\Sigma_i (s_{\rm nom}) N_{D^0,i}}{\Sigma_i N_{D^0,i}}, \tag{6}$$

$$g_{D^+}(s_{\rm nom}) = \frac{\Sigma_i g_i(s_{\rm nom}) N_{D^+,i}}{\Sigma_i N_{D^+,i}}. \tag{7}$$

This procedure results in the corrections shown in Fig. 10. Since neither method models the data precisely, and the two models vary differently with energy, a systematic uncertainty is assigned to be one half the rms difference between the two models over the energy range 3.9 GeV to 4.2 GeV excluding the region from 4.021 to 4.027 where the coupled channel model $D\overline{D}$ cross section is tiny, causing the ISR correction to diverge. The corrections for initial state radiation at $\sqrt{s} = 4.03\,{\rm GeV}$ and $\sqrt{s} = 4.14\,{\rm GeV}$ are

$$4.03\,{\rm GeV}: \quad g_{D^0} = 0.67 \pm 0.05, \tag{8}$$

$$g_{D^+} = 0.73 \pm 0.05, \tag{9}$$

$$4.14\,{\rm GeV}: \quad g_{D^0} = 0.83 \pm 0.06, \tag{10}$$

$$g_{D^+} = 0.84 \pm 0.06. \tag{11}$$

The ISR correction for D_s mesons was calculated using the coupled channel model and the same *P*-wave phase space formalism. Figure 11 shows a prediction for the tree level cross section of D_s and D_s^*, the observed cross section of D_s and D_s^*, the fraction of D_s mesons from direct production, and the fraction of D_s mesons from D_s^* decays. Figure 10(c) shows the ISR correction for D_s mesons. The ISR contribution to the systematic error for D_s production is taken as one half the rms difference between the two models:

$$4.03\,{\rm GeV}: \quad g_{D_s} = 0.73 \pm 0.04, \tag{12}$$

$$4.14\,{\rm GeV}: \quad g_{D_s} = 0.78 \pm 0.05. \tag{13}$$

The ISR and vacuum polarization corrections are applied to the observed D^0 and D^+ cross sections found in Table II to obtain the tree level cross section for D^0 and D^+ at 4.03 GeV and 4.14 GeV as shown below:

$$4.03\,{\rm GeV}: \quad \sigma_{D^0} + \sigma_{\overline{D}^0} = 19.9 \pm 0.6 \pm 2.3\,{\rm nb}, \tag{14}$$

$$\sigma_{D^+} + \sigma_{D^-} = 6.5 \pm 0.2 \pm 0.8\,{\rm nb}, \tag{15}$$

$$4.14\,{\rm GeV}: \quad \sigma_{D^0} + \sigma_{\overline{D}^0} = 9.3 \pm 2.1 \pm 1.1\,{\rm nb}, \tag{16}$$

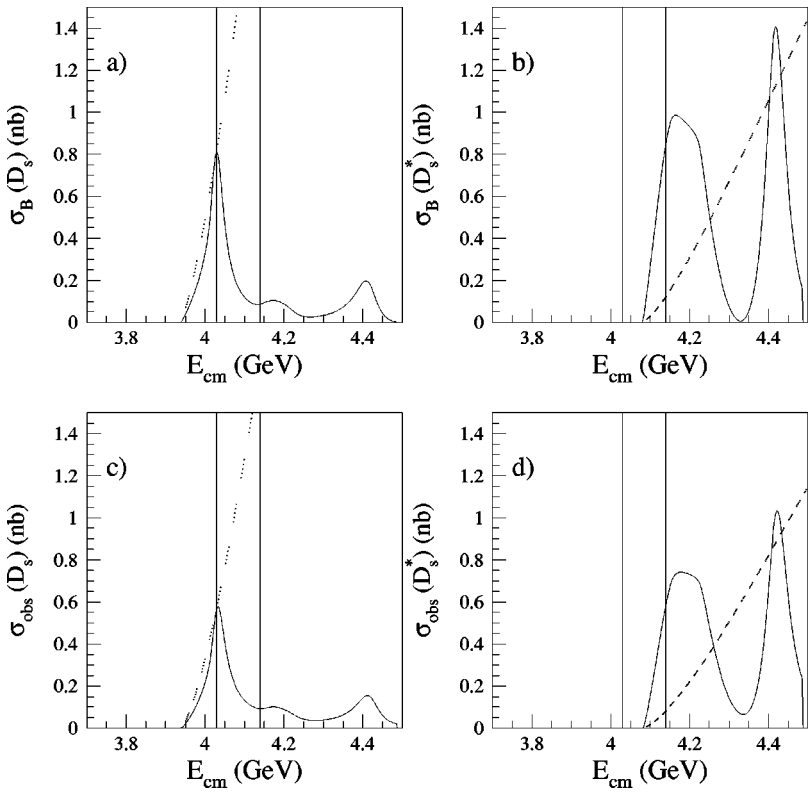

FIG. 11. (a) The tree level cross section for D_s mesons. (b) The tree level cross section for D_s^* mesons. (c) The observed cross section for D_s mesons. (d) The observed cross section for D_s^* mesons. The solid curve was obtained using the coupled channel model. The dashed line was obtained using the *p*-wave phase space formalism.

$$\sigma_{D^+}+\sigma_{D^-}=1.9\pm0.9\pm0.2\,\text{nb}. \tag{17}$$

Systematic uncertainties are treated in Sec. VI.

The BES observed D_s cross section at 4.03 GeV is $\sigma_{D_s^+}+\sigma_{D_s^-}=0.62\pm0.12\pm0.20$ nb [10]. After applying the ISR and vacuum polarization corrections, the tree level D_s cross section is $\sigma_{D_s^+}+\sigma_{D_s^-}=0.81\pm0.16\pm0.27$ nb. The Mark III observations of D_s at 4.14 GeV give $\sigma_{D_s^+}+\sigma_{D_s^-}=1.34\pm0.32\pm0.34$ nb [11]. After correction, the tree level value is $\sigma_{D_s^+}+\sigma_{D_s^-}=1.64\pm0.39\pm0.42$ nb.

VI. SYSTEMATICS

Several systematic checks were performed. The numbers of signal events in the distributions shown in Figs. 1 and 2 were compared to the sum of signal events from each momentum slice as shown in Table III. Good agreement for the 4.03 GeV data validates the slicing technique. For the 4.14 GeV data set, which is much smaller, the agreement is poorer. This could be due to statistical fluctuations.

The analysis was repeated using wrong sign combinations ($K^+\pi^+, K^+\pi^+\pi^-$) to explore systematic bias from the slicing and fitting procedure. As expected, the structures that are so evident in the right sign spectra are absent in the wrong sign spectra (Fig. 12). There is, however, a small excess when the $K^-\pi^-\pi^+$ spectrum is integrated:

$$(\sigma_{D^0}+\sigma_{\bar{D}^0})_{WS}=0.29\pm0.21\,\text{nb}, \tag{18}$$

$$(\sigma_{D^+}+\sigma_{D^-})_{WS}=0.7\pm0.2\,\text{nb}. \tag{19}$$

Both the data and the charged Monte Carlo (MC) simulation show a small excess that was not present in neutral decays. A much larger MC study would be required to prove whether the source is procedural, or if there is a small feed down

TABLE III. Comparison of the number of events found from the inclusive mass fit and the sum of the events from invariant mass fits for the momentum slices.

	$\sqrt{s}=4.03$ GeV		$\sqrt{s}=4.14$ GeV	
	Inclusive D	Sum of slices	Inclusive D	Sum of slices
D^0	4174 ± 163	4232 ± 114	249 ± 36	210 ± 46
D^+	2341 ± 138	2395 ± 94	126 ± 31	66 ± 33

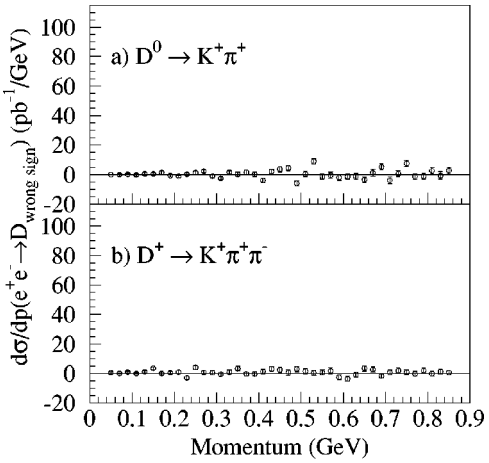

FIG. 12. The differential production cross section for wrong sign combinations.

TABLE IV. Common and independent sources of systematic uncertainty. When summing cross sections for different D species, common uncertainties are added linearly and independent uncertainties are added quadratically.

Common	4.03 D^0	4.03 D^+	4.14 D^0	4.14 D^+	4.03 D_s	4.14 D_s
Luminosity	5%	5%	5%	5%	5%	
D Branching fraction	2.3%	2.3%	2.3%	2.3%		
ISR	7%	7%	7%	7%	6%	6%
Vacuum polarization	2.2%	2.2%	2.2%	2.2%	2.2%	2.2%
Independent	4.03 D^0	4.03 D^+	4.14 D^0	4.14 D^+	4.03 D_s	4.14 D_s
D Branching fraction		6.2%		6.2%		
MC statistics	5%	4%	5%	4%		
Fit parameters	5%	5%	5%	5%		
Previous measurements					31.9%	15.0%

from right sign channels into the wrong sign analysis. If the source of the excess is procedural, the MC efficiency calculation should correct for the effect in the data. In either case, no correction is required.

Systematic errors arising from the choice of parameters were evaluated by repeating the analyses using different bin sizes, fitting ranges, mass resolutions, and background function shapes. Electron particle identification dominates the integrated luminosity uncertainty as determined from wide angle Bhabha scattering events. The uncertainty is evaluated by comparing samples selected independently using dE/dx and the barrel shower counter. In addition there are systematic errors due to the uncertainties in the Monte Carlo–determined reconstruction efficiency, errors in the charmed meson branching fractions, and the uncertainties in the evaluation of the ISR correction scheme as discussed above. Magnitudes of these systematic uncertainties are shown in Table IV.

Sources of systematic uncertainty are segregated into components that are common or independent for D^0, D^+, and D_S measurements. The common components are the integrated luminosity measurement, the ISR correction, the vacuum polarization correction, and a portion of the D branching fraction uncertainties. Since the absolute branching fraction scale for D^+ mesons depends on the D^0 branching fraction scale, the total percentage uncertainty for D^+ branching fraction (6.7%) is split into a common component that matches the percentage uncertainty for the D^0 branching fraction (2.3%) and an independent component (6.2%). All other systematic uncertainties are treated as independent and added in quadrature. Values are found in Table IV.

The total observed D^0 and D^+ cross sections are shown in Table II. Tree level D^0 and D^+ cross sections are shown in Table V.

VII. TOTAL INCLUSIVE CHARM CROSS SECTION

Since all D mesons are produced in pairs, the tree level nonstrange D cross sections are

$$4.03\,\text{GeV}: \quad \sigma(D\bar{D}X) = 13.2 \pm 0.3 \pm 1.4\,\text{nb}, \tag{20}$$

$$4.14\,\text{GeV}: \quad \sigma(D\bar{D}X) = 5.6 \pm 1.1 \pm 0.6\,\text{nb}. \tag{21}$$

Adding the tree level D cross sections to the tree level D_s cross sections gives the total tree level charm cross section:

$$4.03\,\text{GeV}: \quad \sigma_{\text{charm}} = 13.6 \pm 0.3 \pm 1.5\,\text{nb}, \tag{22}$$

$$4.14\,\text{GeV}: \quad \sigma_{\text{charm}} = 6.4 \pm 1.2 \pm 0.7\,\text{nb}. \tag{23}$$

These results are compared to coupled channel model predictions in Table V.

VIII. MEASUREMENT OF R_D AND R

A measurement of R_D is obtained by dividing $2 \times \sigma_{\text{charm}}$ by the QED prediction for the tree level muon pair cross section

$$\sigma(e^+e^- \to \mu^+\mu^-) = \frac{86.8\,\text{nb}}{s(\text{GeV})^2}, \tag{24}$$

giving

$$4.03\,\text{GeV}: \quad R_D = 5.10 \pm 0.12 \pm 0.55, \tag{25}$$

$$4.14\,\text{GeV}: \quad R_D = 2.53 \pm 0.46 \pm 0.27. \tag{26}$$

TABLE V. Comparison of tree level cross section measurements with predictions of the coupled channel model.

$\sqrt{s} = 4.03$ GeV	Experiment	Coupled Channel Model
$\sigma_{D^0} + \sigma_{\bar{D}^0}$	$19.9 \pm 0.6 \pm 2.3$ nb	18.2 nb
$\sigma_{D^+} + \sigma_{D^-}$	$6.5 \pm 0.2 \pm 0.8$ nb	6.0 nb
$\sigma_{D_s^+} + \sigma_{D_s^-}$	$0.81 \pm 0.16 \pm 0.27$ nb	1.61 nb
σ_{charm}	$13.6 \pm 0.3 \pm 1.5$ nb	12.9 nb
$\sqrt{s} = 4.14$ GeV	Experiment	Coupled channel model
$\sigma_{D^0} + \sigma_{\bar{D}^0}$	$9.3 \pm 2.1 \pm 1.1$ nb	15.1 nb
$\sigma_{D^+} + \sigma_{D^-}$	$1.9 \pm 0.9 \pm 0.2$ nb	4.5 nb
$\sigma_{D_s^+} + \sigma_{D_s^-}$	$1.64 \pm 0.39 \pm 0.42$ nb	1.85 nb
σ_{charm}	$6.4 \pm 1.2 \pm 0.7$ nb	10.7 nb

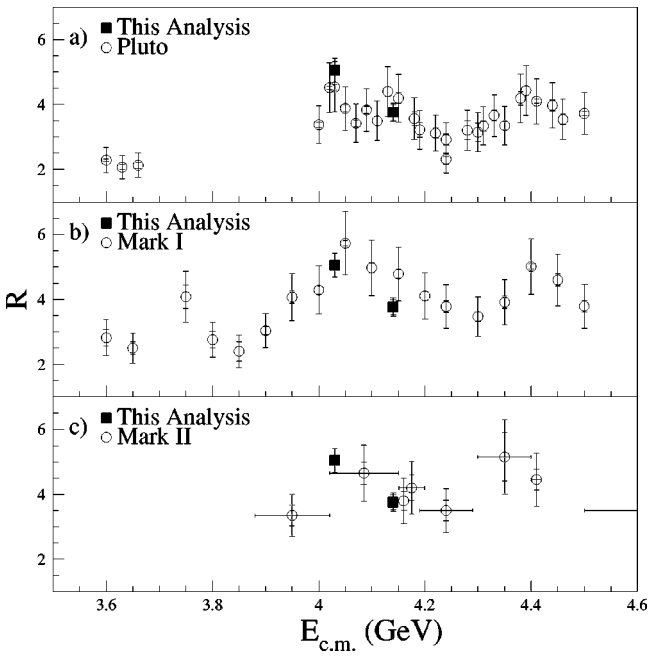

FIG. 13. A comparison of the value of R from this measurement with direct R measurements from Pluto and Mark I and a charm-counting R measurement from Mark II.

The contribution to R in the charm threshold region from the light quarks, R_{uds} is estimated to be 2.5 ± 0.25 [7]. This value was compiled from an average of measurements of R below charm threshold [12–14]. The theoretical expectation is that R_{uds} is approximately independent of center of mass energy in this region. The value of R is evaluated using $R=R_D/2+R_{uds}$ giving

$$4.03\,\text{GeV}: \quad R=5.05\pm0.06\pm0.37, \tag{27}$$

$$4.14\,\text{GeV}: \quad R=3.76\pm0.23\pm0.28. \tag{28}$$

This measurement is more precise, but compatible with previous R measurements [12,14] using the total cross section method shown in Figs. 13(a) and 13(b) and a previous measurement [7] employing a similar R_D technique shown in Fig. 13(c). Charm-counting complements direct R measurements since the two methods feature different systematic uncertainties.

ACKNOWLEDGMENTS

We would like to thank the staffs of the BEPC accelerator and the Computing Center at the Institute of High Energy Physics (Beijing). This work was supported in part by the National Natural Science Foundation of China under Contract No. 19290400 and the Chinese Academy of Sciences under Contract No. KJ85 (IHEP); by the Department of Energy under Contract Nos. DE-FG03-92ER40701 (Caltech), DE-FG03-93ER40788 (Colorado State University), DE-AC02-76ER03069 (MIT), DE-AC03-76SF00515 (SLAC), DE-FG03-91ER40679 (UC Irvine), DE-FG03-94ER40833 (University of Hawaii), DE-FG03-95ER40925 (UT Dallas); by the U.S. National Science Foundation Grant No. PHY9203212 (University of Washington).

[1] M. Swartz, Phys. Rev. D **53**, 5268 (1996).
[2] J. Z. Bai *et al.*, Phys. Rev. D **57**, 3854 (1998).
[3] J. Z. Bai *et al.*, Nucl. Instrum. Methods Phys. Res. A **344**, 319 (1994).
[4] Particle Data Group, R. M. Barnett *et al.*, Phys. Rev. D **54**, 1 (1998).
[5] M. Piccolo *et al.*, Phys. Lett. **70B**, 260 (1977).
[6] M. Piccolo *et al.*, Phys. Lett. **86B**, 220 (1979).
[7] M. W. Coles *et al.*, Phys. Rev. D **26**, 2190 (1982).
[8] E. Eichten *et al.*, Phys. Rev. D **21**, 203 (1980).
[9] E. A. Kuraev and V. S. Fadin, Yad. Fiz. **41**, 733 (1985) [Sov. J. Nucl. Phys. **41**, 466 (1985)]; J. P. Alexander *et al.*, Nucl. Phys. **B320**, 45 (1989).
[10] J. Z. Bai *et al.*, Phys. Rev. D **52**, 3781 (1995).
[11] J. Adler *et al.*, Phys. Rev. Lett. **63**, 1211 (1989); B. Nemati, Ph.D. thesis, University of Washington, 1990; S. Wasserbaech (private communication).
[12] J. Burmeister *et al.*, Phys. Lett. **66B**, 395 (1977).
[13] R. Brandelik *et al.*, Phys. Lett. **76B**, 361 (1978); J. Kirkby *et al.*, in *Weak Interactions–Present and Future*, Proceedings of the SLAC Summer Institute on Particle Physics, 1978, edited by M. Zipf (SLAC, Stanford, 1978).
[14] J. L. Siegrist *et al.*, Phys. Rev. D **26**, 969 (1982).